Discreteness of Charge Effects on the Double Layer Structure at the Metal/Solid Electrolyte Interface

B. R. Horrocks* and R. D. Armstrong

Department of Chemistry, Bedson Building, University of Newcastle upon Tyne, Newcastle upon Tyne, NE1 7RU, UK

Received: July 23, 1999; In Final Form: October 15, 1999

Monte Carlo simulations and analytical approximations for a primitive model of the metal/solid electrolyte interface are presented. The mobile positive and negative point charges in the solid electrolyte are restricted to the corresponding sites of a NaCl lattice (Schottky defects). Single imaging of the mobile charges in the metal was considered. This model of the metal/solid electrolyte interface differs substantially from the primitive model metal/liquid electrolyte interface as a direct result of the discrete spatial locations available to the charges. When the temperature or the dielectric constant of the electrolyte is high, the potential and charge decay monotonically with distance from the interface. The diffuse layer is however less evident than in an analogous primitive model of the metal/liquid electrolyte interface. At high values of the ratio $(qe)^2/T\epsilon$, an oscillation in the charge density profile is observed as in primitive model simulations of liquid electrolytes. This phenomenon is however more marked for solid electrolytes, which can be rationalized in terms of the discrete spatial locations occupied by the charges in the electrolyte. As a direct consequence of the charge oscillation, the interfacial capacitance may exceed the Helmholtz capacitance calculated using the lattice parameters of the solid electrolyte, a phenomenon which has been observed experimentally.[16−18] The Monte Carlo data can be fitted approximately by a simple modification of the Poisson−Boltzmann equation in which an exponentially decaying function of distance proportional to the total interfacial potential drop is added to the potential in the Boltzmann factor.

1. Introduction

The metal/liquid electrolyte interface has been the subject of extensive theoretical and experimental investigations.[1−13] By comparison, the metal/solid electrolyte interface is less well understood. Measurements of the capacitance of metal/single-crystal ionic conductor interfaces became available in the 1970s and showed a different behavior to the metal/liquid electrolyte double layer capacitance. In particular, no diffuse layer minimum in the capacitance (C) − potential (E) curve was often observed[14,15] and in some cases differential capacitances greater than the Helmholtz capacitance were measured.[16−18] Several explanations have been advanced for these observations in terms of disordering of the crystal lattice in the first few lattice planes adjacent to the metal surface or limitations on the charge density which can be accommodated by any lattice plane. Calculations of the consequences of such effects have been made[16,19−22] and conditions under which the diffuse layer minimum in the $C-E$ curve disappears have been demonstrated. However, it should be noted that the discrepancy between the Gouy−Chapman−Stern theory of the double layer and the capacitance data may reflect the approximations involved in the Poisson−Boltzmann equation rather than indicate the need for a more detailed model of the interface. Indeed, it has been well-established from Monte Carlo simulations[23−28] and more accurate statistical mechanical methods[29−36] that the Gouy−Chapman−Stern theory fails qualitatively for highly charged interfaces in electrolytes containing multiply charged ions. In this report, we simulate the metal/solid electrolyte double layer at the same level as the standard primitive model of metal/liquid electrolytes and show that significant differences occur as a result of the restriction of the mobile charges to discrete spatial positions in the solid. In addition, we show that aspects of the experimental data which appear anomalous are in fact present in the simple model of the interface based on mobile defects in an otherwise perfect lattice and their absence in the Gouy−Chapman−Stern theory is due to the mathematical approximations involved.

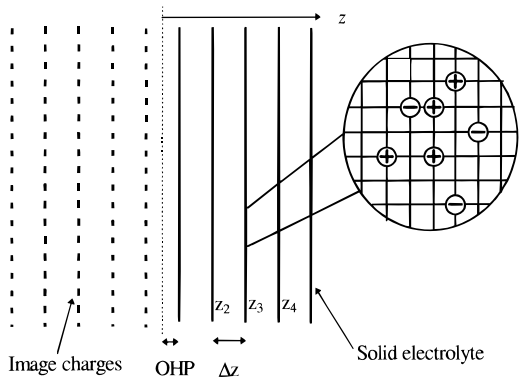

Figure 1. Model of the metal/solid electrolyte interface. The {100} planes of an NaCl lattice are labeled by their distance from the metal surface, z_i.

2. Model

The model of the metal/solid electrolyte interface employed in this study is illustrated in Figure 1. The mobile charges in the solid electrolyte are restricted to the sites of a NaCl lattice corresponding to the situation where the charge carriers are cation and anion vacancies, i.e., Schottky defects. Other cases

10.1021/jp992554y CCC: $18.00
Published on Web 12/04/1999

such as cation vacancies + cation interstitials (Frenkel defects) are also possible; however, they are not treated here since we are primarily interested in the effect of restricting the ions to discrete sites in a lattice as compared to the situation in a fluid. For each real charge in the electrolyte, a corresponding image charge of equal magnitude and opposite sign appears in the metal. The position of the interface is shown in Figure 1 as a dotted line midway between the first lattice planes of real and image charges. The lattice planes are denoted z_i, and z_1 is the plane of closest approach to the metal surface, i.e., the outer Helmholtz plane. In all the calculations, the interface is parallel to the {100} planes of the NaCl lattice. The simulation box consisted of L square lattice planes each containing W^2 sites. The image charges move in an identical box obtained by reflection in the interface. The charges were confined in the direction normal to the interface (ideally polarizable electrode) and by a hard wall far from the interface (typically $L = 50$). The simulation box was replicated in the directions parallel to the interface and the usual minimum image convention was applied. As in the primitive model of the metal/liquid electrolyte interface where the molecular structure of the solvent is ignored, the bulk solid was treated as a lattice of fixed charges and mobile defects in a continuous medium with a uniform dielectric constant, ϵ.

The energy is conveniently calculated with respect to a perfect defect-free crystal. In this case, the internal energy of a particular configuration of this system can be split into three terms:

$$U(r) = \sum_{i<j} u(r_i,r_j) + \sum_i v(z_i) + \sum_i \Gamma(z_i) \qquad (1)$$

Where i and j label individual vacancies which are treated as additional mobile charges of equal magnitude and opposite sign to the fixed ion at the same lattice point (Figure 1). The first term in eq 1 is the pairwise Coulomb interaction between all these charges including image charges. The restriction on the sum avoids overcounting the interactions between real charges and takes account of the work done in forming the image charges.[37]

$$u(r_i,r_j) = \frac{q_i q_j e^2}{4\pi\epsilon\epsilon_0}\left[\frac{1}{r_{ij}} - \frac{1}{r'_{ij}}\right] \qquad (2)$$

Where r_{ij} and r'_{ij} are the minimum image distances between pairs of real charges of magnitude $q_i e$ and $q_j e$ and the corresponding image charges.

The second term in eq 1 includes the interaction of a charge with its own image at $-z_i$ and also with a smeared out charge density (σ_j) on all the lattice planes in the region outside the simulation box via the potential, $\Phi(z_i)$.

$$v(z_i) = \frac{1}{2}\frac{q_i^2 e^2}{8\pi\epsilon\epsilon_0 z_i} + q_i e\Phi(z_i) \qquad (3)$$

The potential, $\Phi(z_i)$, was calculated from the mean charge density on each lattice plane and each plane of images integrated over the area outside the simulation box and was updated during the simulation as described by Torrie and Valleau.[37]

Finally, the third term describes the energy required to create a mobile charge (i.e., vacancy) at z_i owing to the electrostatic interactions with the fixed charges (at jkl) that form the bulk solid. This term is not important when $z_1 = \Delta x/2$ since the contribution to the energy is then independent of z_i. This situation would occur when the atoms of the electrolyte and the metal have equal radii and is the case treated in most of the simulations described in this paper. However if $z_1 > \Delta x/2$, the larger average distance between a charge in the first lattice plane and its nearest neighbors leads to a lower internal energy of formation for a vacancy at z_1 compared to the bulk.

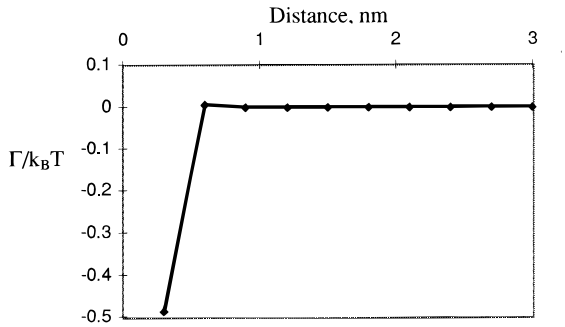

Figure 2. Internal energy required to create a vacancy, $\Gamma k_B T$, against distance from the metal/solid electrolyte interface. The lattice parameter $\Delta z = z_1 = 0.3$ nm, the dielectric constant = 25 and $T = 298$ K.

$$\Gamma(z_i) = |q_i| e f(z_i) \qquad (4)$$

with

$$f(z_i) = \sum_{j=-\infty}^{\infty}\sum_{k=-\infty}^{\infty}\sum_{l=-\infty}^{\infty} \frac{-1^{j+k+l}}{4\pi\epsilon\epsilon_0}\left(\frac{e}{r_{ijkl}} - \frac{e}{r'_{ijkl}}\right)$$

$$r_{ijkl} = \sqrt{(j\Delta x)^2 + (k\Delta x)^2 + (z_i - (l-1)\Delta x - z_1)^2}$$

$$r'_{ijkl} = \sqrt{(j\Delta x)^2 + (k\Delta x)^2 + (z_i + (l-1)\Delta x - z_1)^2}$$

Since this term depends only on z_i, the triple sum was evaluated directly at the start of the simulation and the values of $f(z_i)$ stored in memory. A cutoff of $-30 < j, k < 30$, and $1 < l < 60$ was found to give adequate accuracy. The magnitude of this effect is illustrated in Figure 2 for the case $z_1 = \Delta z$. This contribution to the internal energy is characteristic of the crystalline ionic solid electrolyte and does not have an analogue in the primitive model liquid electrolyte.

3. Simulation and Data Analysis

Both canonical Monte Carlo (CMC) and Grand Canonical Monte Carlo (GCMC) simulations were run with n_+ mobile positive charges and n_- mobile negative charges in the simulation box and a fixed excess charge ($n_+ - n_-$) on the electrolyte. In the latter case, creation and destruction moves were applied to neutral pairs of charges (i.e., vacancies) to ensure that the total charge was fixed throughout the simulation. The activity was input as a free parameter and the resulting bulk electrolyte concentration was calculated at the end of the simulation from the accumulated charge and ion density profiles. The density profile of positive and negative ions normal to the interface was updated every $n_+ + n_-$ attempted moves and used in the computation of internal energy via eq 4. The simulations were run at various box sizes and for various numbers of steps to check for convergence. Averages were collected over 10^4 to 3×10^4 moves/particle and the uncertainties were estimated by the block average method.[38] Several runs were made with different excess charge and either a fixed value of n_- (CMC) or with a fixed activity (GCMC). The potential drop across the interface was then calculated by integration of the field obtained from the in-plane space-averaged charge density profile. The

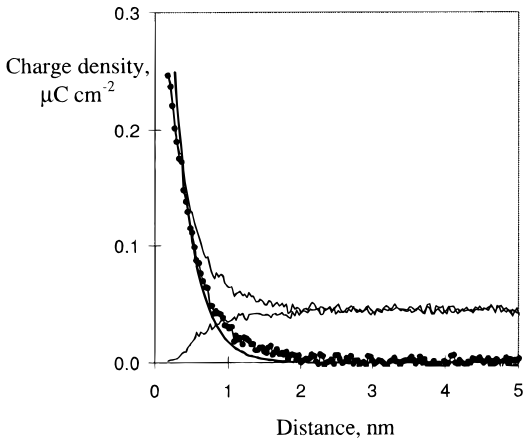

Figure 3. Density profiles from a CMC simulation of a liquid electrolyte. Net charge (●), counterion and coion profiles (−), and the Gouy−Chapman−Stern model prediction for net charge (—). Δz = 0.3 nm, z_1 = 0.15 nm, T = 298 K and dielectric constant = 25. The bulk electrolyte concentration was 0.123 mol dm^{-3}.

potential-distance profiles are presented with symbols connected by straight lines as is the case for point charges. However, if the ionic charges were considered to be distributed over a sphere centered at the lattice point, the charge distribution would be modified and a smooth potential profile would be obtained. Since this correction would depend somewhat on the electronic structure of the ions we have not attempted to calculate it here. In CMC simulations, small deviations of the charge density from zero at large distances from the interface produced a significant effect on the calculated potential. A small offset was therefore added or subtracted from the charge density profile to center the charge density at zero, far from the interface where the charge density profile was observed to be flat. The offset was <1% of the charge at z_1. This effect was negligible in the GCMC simulations, and no correction was required. Series of simulations at fixed conditions, but increasing charge density, were used to construct charge density−electrode potential plots, and the interfacial capacitance was estimated from a least-squares polynomial fit to these plots.

4. Results and Discussion

To test the simulation algorithm, we initially allowed the charges to move freely throughout the electrolyte with a hard sphere diameter of Δz. This corresponds to a primitive model metal/liquid electrolyte interface. Figure 3 shows the equilibrium space-averaged charge density profile normal to the interface which was reasonably well described by the Gouy−Chapman−Stern theory for potentials near the potential of zero charge (pzc). However, when the charges are restricted to occupation of discrete lattice sites the charge density profile is much steeper and the diffuse layer is less evident (Figure 4). This effect is not observed when the charge in each lattice plane is treated as smeared-out[22] and therefore appears to be a result of the discreteness of charge in-plane.

At low electrode potentials, CMC and GCMC simulations were in agreement although the former converged more rapidly. However, as the charge on the electrode increased, the two types of simulation produced significantly different results. This arises because the finite size of the simulation box normal to the interface means that the system being simulated is really metal/electrolyte/insulator. In the case of the CMC method where the total numbers of each ion in the simulation box is fixed, the rejection of coions from the metal surface causes a significant

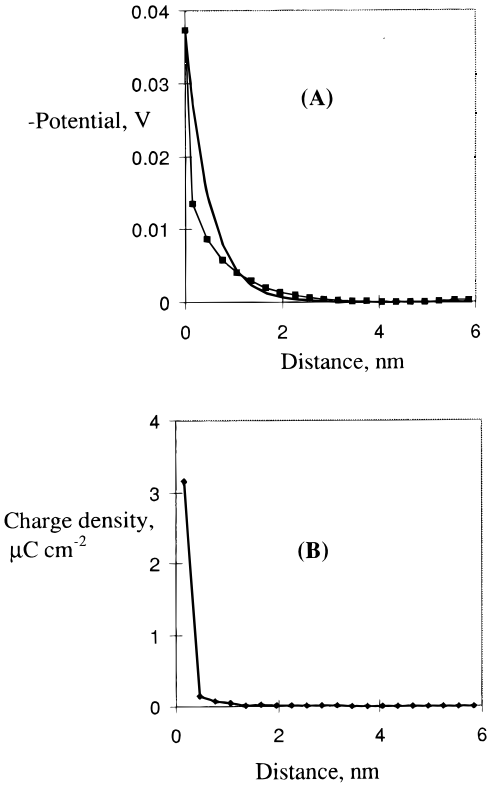

Figure 4. Equilibrium space-averaged potential against distance (A) and net charge density against distance (B) for a GCMC simulation of the metal/solid electrolyte interface. Δz = 0.3 nm, z_1 = 0.15 nm, T = 298 K, and dielectric constant = 25. The bulk electrolyte concentration was 0.086 mol dm^{-3}. The solid line in (A) was calculated from the Gouy−Chapman−Stern theory.

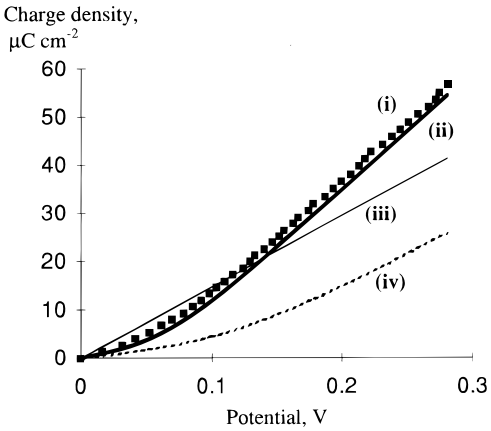

Figure 5. Metal charge density against electrode potential. Δz = 0.3 nm, z_1 = 0.15 nm, T = 298 K, and dielectric constant = 25. The bulk electrolyte concentration was 0.089 mol dm^{-3}: (i) GCMC simulation; (ii) calculated according to the approximate theory of eq 9; (iii) according to Helmholtz model; (iv) according to the Gouy−Chapman−Stern model.

change in the concentration of coions throughout the simulation box at high electrode potentials. As is well-known, the GCMC method avoids this problem since the interface is in equilibrium with bulk electrolyte of fixed activity.

Figure 5 shows that the charge−potential plot lies above that calculated from the Gouy−Chapman−Stern theory at all potentials. In addition, the Q−E plot crosses the line drawn to show the charge density expected for the Helmholtz model of the double layer, $Q = (\epsilon\epsilon_0/z_1)E$. At potentials where the interfacial capacitance exceeds $\epsilon\epsilon_0/z_1$, the charge and ion density

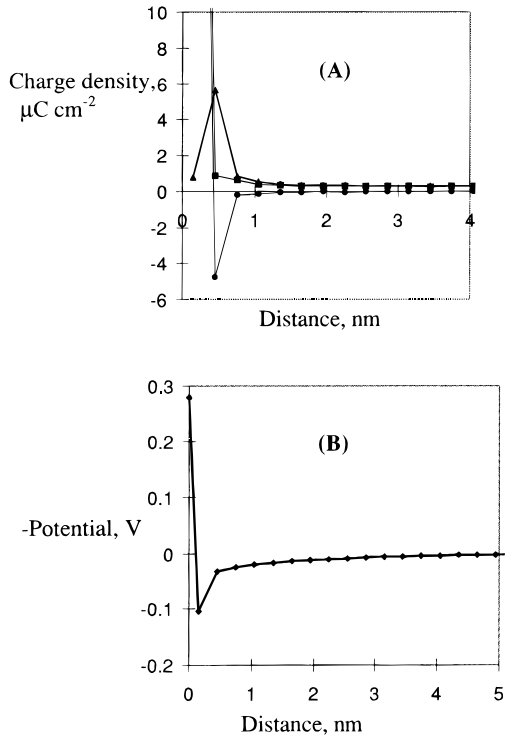

Figure 6. (A) Net charge (●), counterion (■), and coion (▲) density profiles from GCMC simulation. (B) Corresponding equilibrium space-averaged potential distribution. $\Delta z = 0.3$ nm, $z_1 = 0.15$ nm, $T = 298$ K, and dielectric constant = 25. The bulk electrolyte concentration was 0.089 mol dm^{-3}.

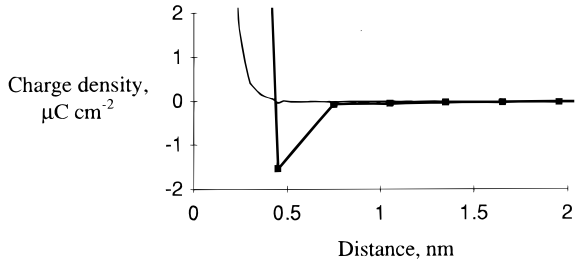

Figure 7. Net charge density against distance for a liquid electrolyte [—] and a solid electrolyte double layer [—■—] under identical conditions: $\Delta z = 0.3$ nm, $z_1 = 0.15$ nm, $T = 298$ K, and dielectric constant = 25. The bulk electrolyte concentration was 0.092 mol dm^{-3}. Metal charge = -31.3 μC cm^{-2}.

profiles (Figure 6) show an oscillation. In this situation, the charge on the electrode is overcompensated by counterions at z_1 and the concentration of coions exceeds the concentration of counterions in subsequent lattice planes. A strong peak in the coion density occurs in the second lattice plane at z_2. A similar phenomenon has been reported previously in calculations on liquid electrolytes with high values of $(qe)^2/T\epsilon$, i.e., multiply charged ions, and/or low temperatures or dielectric constants. The origin of the effect for liquid electrolytes has been described in detail.[13] However, we observed that the oscillation is more pronounced in our model solid electrolyte, where point charges are restricted to occupy discrete sites. Although the charge oscillation still requires a large value of the coupling constant, $(qe)^2/T\epsilon$, simulations of liquid and solid electrolytes at identical values of the coupling constant can show a marked difference. An example is shown in Figure 7 where the charge oscillation is barely visible in the liquid case (line), but quite distinct in the solid case (bold line + symbols), though the difference between the solid and liquid cases would be smaller if the charge

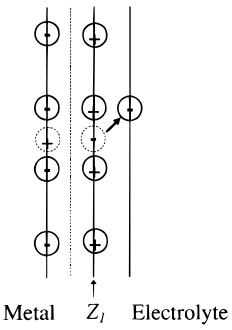

Figure 8. Schematic illustration of the origin of the peak in the coion density profile at the second lattice plane (negative charges in this illustration).

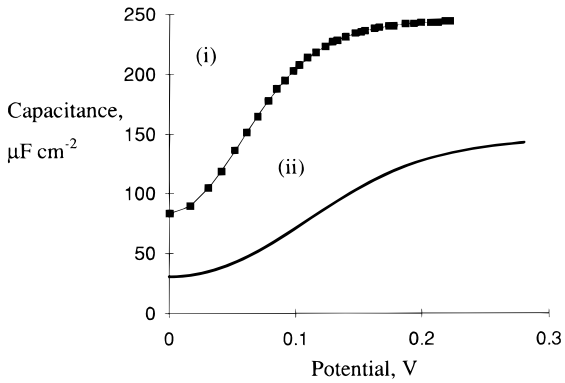

Figure 9. Capacitance—potential curves: (i) calculated from the simulation of Figures 5 and 6; (ii) Gouy—Chapman—Stern model. $\Delta z = 0.3$ nm, $z_1 = 0.15$ nm, $T = 298$ K, and dielectric constant = 25. The bulk electrolyte concentration was 0.089 mol dm^{-3}.

were distributed throughout a spherical model ion in the solid. Figure 8 indicates schematically our interpretation. The coions at z_1 feel a force normal to the interface from the excess charge on the metal surface. In a liquid electrolyte, these coions would be able to take up a continuous range of positions further from z_1. In contrast, coions in the solid electrolyte will accumulate in the next-nearest available sites in the second lattice plane where the counterions at z_1 effectively screen the charge on the metal. A similar effect may be occurring in the recent simulations of a fluid mixture of charged and dipolar hard spheres where the dipolar spheres model the solvent and introduce a layered structure near the electrode.[28] If the interface is considered as two capacitors in series, the sign of the potential dropped between z_1 and z_2 is opposite to that between the metal and z_1. The total potential dropped across the interface is therefore smaller than in the absence of the charge oscillation and the interfacial capacitance is therefore greater than in the Helmholtz model where the counterions at z_1 do not overcompensate the charge on the metal. The capacitance calculated from the GCMC simulations of Figures 5 and 6 is compared with the Gouy—Chapman—Stern model in Figure 9. Although the relative depth of the diffuse layer minimum is smaller and the minimum is narrower in the simulation, a minimum is still clearly present within 100 mV of the potential of zero charge. The discreteness-of-charge effect does not therefore account completely for the absence of the diffuse layer minimum in the experimental data and other factors which have been suggested such as an increased carrier concentration at the interface due to disorder in the first few lattice planes or a potential of zero charge (pzc) outside the potential window may well be present in the experimental systems.[14,16] However, it is clear that the cases[16—18] where the measured capacitance is of the order of

TABLE 1: Simulation Data[a]

run no.	c/mol dm^{-3}	T^*	E/V	Q	$Q1$	$Q2$
(a) GCMC	$4.2(4) \times 10^{-1}$	0.134	0.053(1)	8.94	−9.5(8)	0.8(4)
(b) GCMC	$6.2(1) \times 10^{-1}$	0.134	0.050(7)	8.94	−9.8(0)	1.0(3)
(c) GCMC	$2.(2) \times 10^{-1}$	0.077	0.1(6)	30.9	−3(4)	2.(6)
(d) GCMC	$2.2(3) \times 10^{-1}$	0.134	0.18(7)	30.9	−31.(9)	0.8(5)
(e) GCMC	$2.2(3) \times 10^{-1}$	0.268	0.30(5)	30.9	−27.(4)	−1.9(4)
(f) CMC	9.23×10^{-2}	0.077	0.088(1)	9.0(0)	−8.1(3)	−0.4(4)
(g) CMC	9.23×10^{-2}	0.111	0.096(7)	8.9(1)	−8.1(0)	−0.3(0)
(h) CMC	9.23×10^{-2}	0.161	0.13(1)	8.9(7)	−7.0(8)	−0.8(1)
(i) CMC	9.23×10^{-2}	0.232	0.16(3)	8.9(5)	−5.9(2)	−1.3(0)
(j) CMC	9.23×10^{-2}	0.279	0.19(0)	8.9(2)	−5.3(7)	−1.4(5)

[a] $\Delta z = 0.3$ nm and $z_1 = 0.15$ nm in all cases, CMC and GCMC denote canonical Monte Carlo and grand canonical Monte Carlo simulations, respectively. $T^* = 4\pi\epsilon\epsilon_0 kT\Delta z/e^2$. Q, $Q1$, and $Q2$ denote the charge on the metal, first (z_1) and second lattice planes (z_2) in μF cm^{-2}. E is the total potential dropped across the interface, and c is the bulk electrolyte concentration. Uncertain digits are bracketted.

10^2 μF cm^{-2} can in principle be accounted for by the primitive model described here.

Selected simulation data are given in Table 1. In general, good results were obtained from simulations with the reduced temperature, $T^* = 4\pi\epsilon\epsilon_0 kT\Delta z/e^2$, having values ≥ 0.1, otherwise the system became stuck in particular configurations. The charge inversion gradually disappears as the temperature is raised. A related simulation[27] pertaining to the metal/molten salt interface showed evidence for the experimentally observed positive temperature coefficient of the capacitance, however this was not observed for the solid electrolyte case simulated here. In solid electrolytes, the experimental data may well reflect thermal generation of mobile charges in the bulk which is not treated by the model used in this paper.

5. Analytical Approximations

In this section, we present some analytical approximations that describe the effects observed in the simulations of restricting the electrolyte charges to (i) lattice planes and (ii) discrete lattice sites.

5.i. Charges Confined to Discrete Planes, but In-Plane the Charge Distribution is Treated as Continuous. The case where the charge in a lattice plane may be treated as though it were smeared-out and can be represented by a charge density, σ_i, has been previously treated numerically.[19−22] The charge density on each plane can be determined from the Boltzmann factor for the mean electrostatic energy required to bring a charge to that plane from infinity. This leads to a difference equation which is equivalent to a particular finite-difference representation of the usual Poisson−Boltzmann equation for continuous media:

$$\frac{\theta_i - \theta_{i-1}}{\Delta z} = -k^2\Delta z\sum_i^{\infty}\sinh\theta_i \qquad (5)$$

Where k is the reciprocal Debye length, $\theta_i - e\phi_i/k_BT$ is the normalized electrostatic potential at the lattice plane i, and $z_1 = \Delta z$. If the left- and right-hand sides are replaced by the corresponding derivative and integral plus correction terms of order Δz^2 in the Taylor series, the following equation is obtained:

$$\frac{\Delta z}{2}\frac{\partial^3\theta}{\partial z^3} + \frac{\partial^2\theta}{\partial z^2} - \frac{\Delta z k^3\cosh\theta}{2}\frac{\partial\theta}{\partial z} - k^2\sinh\theta = 0 \qquad (6)$$

Where the terms containing the lattice spacing, Δz, account for the effects of discretisation in the direction normal to the interface. An extra boundary condition is required to solve (6) which is the absence of charge at $z = 0$ on the electrolyte side of the interface before the first lattice plane. At low potentials, the equation may be linearized and solved to obtain

$$\theta = \theta_0\left(\frac{4}{4 - k^2\Delta z^2}e^{-kz} + \frac{k^2\Delta z^2}{k^2\Delta z^2 - 4}e^{-2z/\Delta z}\right) \qquad (7)$$

which gives for the capacitance at the pzc

$$C_{pzc} = \frac{2k\epsilon\epsilon_0}{2 + k\Delta z} \qquad (8)$$

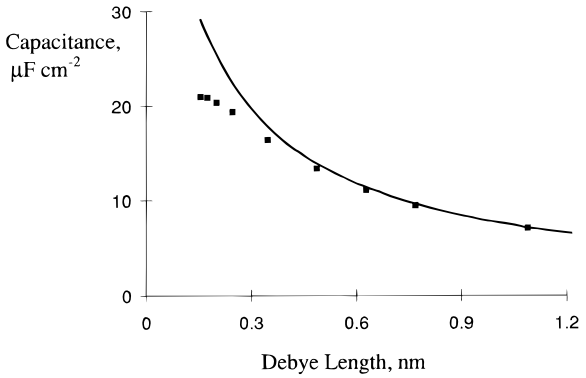

Figure 10. Double layer capacitance versus Debye length for a constant lattice plane spacing of 0.3 nm and a continuous charge distribution in-plane. The symbols were obtained from the numerical solution of eq 5 as described previously[22] and the line is the approximation given in eq 8.

Figure 10 shows a plot of the capacitance at the pzc obtained from numerical solution of the Poisson−Boltzmann difference eq 5 for the case where $z_1 = \Delta z$ with the approximation of eq 8. The approximation is reasonable for values of Δz that are not too large compared to the Debye length. The capacitance near the pzc is slightly increased compared to the Gouy−Chapman−Stern theory. The potential distribution according to eq 7 lies above the Gouy−Chapman exponential decay. The effect of discretisation on the potential distribution resembles qualitatively the excluded volume corrections to the Gouy−Chapman model of the double layer in fluid electrolytes due to the hard core repulsions between ions and solvent molecules.[19,39,40]

5.ii. Charges Confined to Discrete Lattice Sites. Numerical solution of eq 6 gives a monotonic variation of the equilibrium space-averaged potential with distance and does not account for the charge inversion and potential oscillation observed in the simulations at high electrode potentials. It is clear also from the form of eq 5 that it does not have solutions as observed in Figure 6, where θ crosses the axis, reaches a minimum, and then decays to zero at large distances. There have been several reports describing the detailed origin of this charge oscillation phenomenon at primitive model double layers in liquid electrolytes,[23−28] and in liquid electrolytes it can be described by more sophisticated theories.[29−36] In the case of the metal/solid electrolyte interface, the oscillation is enhanced (see Figure 7) because those coions which are rejected from z_1 due to the unscreened charge on the metal are forced to occupy sites in the second lattice plane since there are no intermediate positions (Figure 8). This effect can be simply, albeit crudely, modeled by the incorporation of an extra term in the Poisson−Boltzmann equation:

$$\frac{\partial^2\theta}{\partial z^2} = k^2 \sinh(\theta + \theta_0 e^{-2z/z_2}) \quad (9)$$

where z_2 denotes the distance of the second lattice plane from the interface and θ_0 is the total potential dropped across the interface. The extra term is large close to the surface and tends to repel coions from the interface. Since the additional term augments the attraction between the counterions and the electrode, eq 11 also reproduces the results of Figure 4 in which the charge and potential decay more rapidly with distance than the Gouy−Chapman−Stern prediction when the interface is close to the pzc. As the electrode potential increases, the charge on the electrode is eventually overcompensated by ions at z_1 and an oscillation in the potential and charge profiles occurs. Equation 9 was solved numerically by the finite difference method on an exponentially expanding grid using successive over-relaxation to solve the difference equations.[41] Figure 11 compares the solution to eq 9 and the potential from the simulation. A qualitative fit to the simulation is observed. In addition, the charge−electrode potential curve can be calculated if the additional assumption is made that there is no charge in the region $0 < z < z_1$. A successful fit to the Monte Carlo data is obtained as shown in Figure 5, although electrode charge calculated from eq 10 is slightly, but significantly, lower than the simulation over the range of potentials investigated. With a suitable choice of z_2, eq 9 may also be of use for modeling systems containing fluid electrolytes where computational speed is important. The temperature dependence of the capacitance predicted from eq 9 also follows the simulations and is negative, in agreement with Gouy−Chapman−Stern theory, although both disagree with some experiments.[15,16]

Equation 9 cannot however model accurately the density profiles of the counterions and coions in the solid since as can be seen directly from their form in Figure 6; the potential of mean force is different for counterions and coions when the electrode charge is finite. It should also be noted that the effect of the vacancy formation energy, Γ, has not been considered here. In the case where $z_1 > \Delta z/2$ this would favor an increase in the concentration of both counterions and coions at z_1 and a decrease at z_2. The simulation shows an increase in the charge density on z_1, and a decrease in the coion peak in the second lattice plane at z_2 for the case $z_1 = \Delta z$ (Figure 12).

6. Conclusions

The metal/solid electrolyte interface differs from typical metal/liquid electrolyte interfaces as a result of the absence of solvent, the discrete spatial locations of the mobile charges, and the low dielectric constants of solid electrolytes. Even when the two interfaces are simulated at the level of the primitive model, striking differences are observed. The combination of low dielectric constant and restriction of electrolyte charges to discrete sites in a lattice leads to a partial suppression of the diffuse layer at the metal/solid electrolyte interface. This finding is qualitatively in agreement with the absence of a diffuse layer minimum in much of the experimental capacitance data for metal/crystalline solid interfaces.

At high electrode potentials, the charge density profile and the potential profile show an oscillation which has previously been described at metal/liquid electrolyte interfaces. In the case of the metal/solid electrolyte interface, the oscillation appears to be more pronounced and this can be traced also to the restriction of mobile charges to occupation of discrete sites. Coions rejected from z_1 owing to the repulsion from charges on the metal electrode which is not screened by counterions

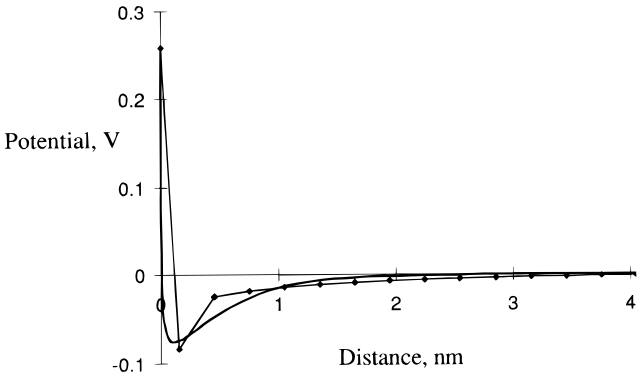

Figure 11. A comparison of the solution of eq 9 {bold line} and the equilibrium space-averaged potential−distance profile for a GCMC simulation {line-symbols}. $\Delta z = 0.3$ nm, $z_1 = 0.15$ nm, $T = 298$ K, and dielectric constant = 25. The bulk electrolyte concentration was 0.089 mol dm^{-3}.

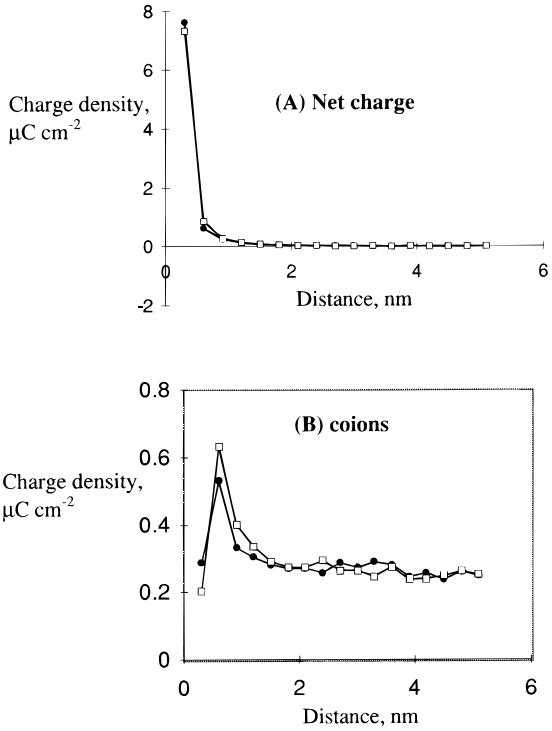

Figure 12. (A) Net charge and coion density profiles from GCMC simulation. $\Delta z = 0.3$ nm, $z_1 = 0.3$ nm, $T = 298$ K and dielectric constant = 25. The bulk electrolyte concentration was 0.089 mol dm^{-3}. (□) indicates that Γ, eq 4,was not included in the calculation; (●) shows the effect of including the vacancy formation energy term, Γ.

accumulate in the next nearest lattice site. For the NaCl lattice, this is exactly one lattice plane distant and a peak in the coion density profile appears here. This phenomenon is revealed in the $C-E$ curve as an interfacial capacitance substantially greater than the Helmholtz capacitance computed from the lattice spacing and the dielectric constant and is consistent with the high capacitance observed experimentally on platinum/silver halogenide[17,18] and silver/yttrium−zirconium oxide interfaces.[16] A modification to the Poisson−Boltzmann equation is described which reproduces the gross behavior of the model metal/solid electrolyte interface without significantly increasing the computational cost.

Acknowledgment. Professors J. Jamnik and J. Maier are acknowledged for drawing our attention to some of the early work in this field.

References and Notes

(1) Barlow, C. A., Jr.; Macdonald, J. R. *Adv. Electrochem. Electrochem. Eng.* **1967**, *6*, 1.
(2) Gouy, G. *J. Phys. Radium* **1910**, *9*, 457.
(3) Chapman, D. L. *Philos. Mag.* **1913**, *25*, 475.
(4) Stern, O. Z. *Electrochem.* **1924**, *30*, 508.
(5) Henderson, D. In *Progress in Surface Science*; Davison, S. G., Ed.; Pergamon Press: Oxford, 1983; Vol. 13, pp 197−224.
(6) Payne, R. *J. Electroanal. Chem.* **1973**, *41*, 277.
(7) Parsons, R. *Rev. Pure Appl. Chem.* **1968**, *18*, 91.
(8) Macdonald, J. R. *J. Electroanal. Chem.* **1987**, *223*, 1.
(9) Spohr, E. *Electrochim. Acta* **1999**, *44*, 1697.
(10) Ritchie, I. M.; Bailey, S.; Woods, R. *Adv. Coll. Int. Sci.* **1999**, *80*, 183.
(11) Kizhakevariam, N.; Villegas, I.; Weaver, M. J. *J. Phys. Chem.* **1995**, *99*, 7677.
(12) Stuve, E. M.; Kizhakevariam, N. *J. Vac. Sci. Technol. A* **1993**, *11*, 2217.
(13) Kjellander, R.; Greberg, H. *J. Electroanal. Chem.* **1998**, *450*, 233.
(14) Armstrong, R. D.; Mason, R. *J. Electroanal. Chem.* **1974**, *41*, 231.
(15) Remez, I. D. *Sov. Electrochem.* **1982**, *18*, 1481.
(16) Chebotin, V. N.; Remez, I. D.; Solovieva, L. M.; Karpachev, S. V. *Electrochim. Acta* **1984**, *29*, 1381.
(17) Raleigh, D. O.; Crowe, H. R. *J. Electrochem. Soc.* **1971**, *118*, 79.
(18) Remez, I. D.; Chebotin, V. N.; Solovieva, L. M.; Karpachev, S. V. *Electrokhimia* **1975**, *11*, 644.
(19) Kenkel, S. W.; Macdonald, J. R. *J. Chem. Phys.* **1984**, *81*, 3215; **1984**, *80*, 2168.
(20) Macdonald, J. R.; Francheschetti, D. R.; Lehnen, A. P. *J. Chem. Phys.* **1980**, *73*, 5272.
(21) Jamnik, J.; Maier, J.; Pejovnik, S. *Solid State Ionics* **1995**, *75*, 51.
(22) Armstrong, R. D.; Horrocks, B. R. *Solid State Ionics* **1997**, *94*, 181. Note: several of the models discussed in this reference were treated previously by Macdonald and co-workers; see, e.g., ref 19.
(23) Sjostrom, L.; Akesson, T.; Jonsson, B. *Ber. Bunsen-Ges. Phys. Chem.* **1996**, *100*, 889.
(24) Degreve, L.; Lozada-Cassou, M. *Phys. Rev. E.* **1998**, *57*, 2978.
(25) Guldbrand, L.; Jonsson, B.; Wennerstrom, H.; Linse, J. *J. Chem. Phys.* **1984**, *80*, 2221.
(26) Svensson, B.; Jonsson, B.; Woodward, C. E. *J. Phys. Chem.* **1990**, *94*, 2105.
(27) Boda, D.; Henderson, D.; Chan, K.-Y. *J. Chem. Phys.* **1999**, *110*, 5346.
(28) Boda, D.; Chan, K.-Y.; Henderson, D. *J. Chem. Phys.* **1998**, *109*, 7362.
(29) Kjellander, R. *Ber. Bunsen-Ges. Phys. Chem.* **1996**, *100*, 894 and references therein.
(30) Outhwaite, C. W.; Bhuiyan, l. B. *J. Chem. Soc., Faraday Trans.* **1983**, *79*, 707 and references therein.
(31) Mier-y-tieran, L.; Suh, S. H.; White, H. S.; Davis, H. T. *J. Chem. Phys.* **1990**, *92*, 5087.
(32) Biben, T.; Hansen. J−P.; Rosenfeld. Y. *Phys. Rev.* **1998**, *57*, R3727.
(33) Carnie, S. L.; Chan, D. Y. C. *J. Chem. Phys.* **1980**, *73*, 2949.
(34) Blum, L.; Henderson, D. *J. Chem. Phys.* **1981**, *74*, 1902.
(35) Coalson, R. D.; Walsh, A. M.; Duncan, A.; Ben-Tal, N. *J. Chem. Phys.* **1995**, *102*, 4584. Coalson, R. D.; Duncan, A. *J. Chem. Phys.* **1992**, *97*, 5653.
(36) Netz, R. R.; Orland, H. *Europhys. Lett.* **1999**, *45*, 726.
(37) Torrie, G. M.; Valleau, J. P. *Chem. Phys. Lett.* **1979**, *65*, 343. Torrie, G. M.; Valleau, J. P. *J. Chem. Phys.* **1980**, *73*, 5807. Torrie, G. M.; Valleau, J. P.; Patey, G. N. *J. Chem. Phys.* **1982**, *76*, 4615.
(38) Allen, M. P.; Tildesley, D. J. *Computer Simulation of Liquids*; Clarendon Press: Oxford, UK, 1987; Chapter 6.
(39) Borukhov, I.; Andelman, D.; Orland, H. *Phys. Rev. Lett.* **1997**, *79*, 435.
(40) Lue, L.; Zoeller, N.; Blankschtein, D. *Langmuir* **1999**, *15*, 3726.
(41) Press, W. H.; Teukolsky, S. A.; Vetterling, W. T.; Flannery, B. P. *Numerical Recipes in Fortran; The Art of Scientific Computing*, 2nd ed.; Cambridge University Press: Cambridge, UK, 1992.